JOURNAL OF PROPULSION AND POWER
Vol. 16, No. 6, November–December 2000

Numerical Study of Fuel Mixing Enhancement Using an Oblique Shock/Vortex Interaction

Ashish Nedungadi* and Mark J. Lewis†
University of Maryland, College Park, Maryland 20742-3015

The effects of swirl and jet-to-freestream pressure ratio on the mixing performance of a swirling helium jet interacting with an oblique shock are investigated. The three-dimensional parabolized Navier–Stokes equations are solved to simulate the parallel injection of a swirling helium jet at Mach 3 into a coflowing stream of air at Mach 4. The effects of swirl and jet-to-freestream pressure ratios on the mixing performance are studied by considering various strengths for the swirling jet and various jet exit pressures, respectively. The mixing performance is based on several parameters that include the maximum helium mass fraction decay, the fraction of total helium mass flux present at various concentrations, and the total entropy rise. It is shown that the fraction of total helium mass flux that is present at $c_{\mathrm{He}} \leq 0.05$ increases from 8 to 16% and that the point at which pure helium ceases to exist occurs farther upstream with the addition of swirl. Furthermore, it is shown that the jet with the lower pressure and momentum provides better mixing performance than the higher pressure jet.

Nomenclature

A	=	area of jet, m^2
c_{He}	=	helium mass fraction
E	=	enstrophy, m^2/s^2
M	=	Mach number
$\dot{m}$	=	mass flow, kg/s
$\bar{p}$	=	nondimensional pressure, p/p_∞
R_j	=	radius of injected jet, m
S	=	swirl number, $\Gamma_0/V_j r_c$
$\bar{V}$	=	nondimensional velocity, V/V_∞
$\bar{X}, \bar{Y}, \bar{Z}$	=	nondimensional coordinates, $[XYZ]/R_j$
Γ_0	=	circulation, m^2/s
ρ	=	density, kg/m^3
τ	=	$V_{\theta,\max}/V_j$

Subscripts

i	=	species
j	=	jet conditions
x	=	streamwise component
∞	=	freestream conditions

Introduction

A CANDIDATE propulsion system for a hypersonic vehicle designed for flight Mach numbers in excess of six will likely be the supersonic combustion ramjet (scramjet). One of the major problems that plagues the design of scramjet engines is achieving successful mixing and burning of the fuel in the combustor in supersonic flow. Typical combustor Mach numbers in these types of engines will be between 2 and 8, depending on the flight Mach number. Consequently, the time available in which the fuel, most likely hydrogen above Mach 8, must be injected, mixed, and burned is only on the order of a few milliseconds. To complicate matters further, as the combustor Mach number increases, the level of mixing through natural convective and diffusive processes decreases.[1] Because the efficiency of the combustion of hydrogen and air is highly dependent on the level to which they are mixed, it is clear that the mixing of the two streams must be achieved as rapidly as possible.

Several injection strategies, including normal injection, parallel injection, and angled injection have been considered. Normal injection can provide rapid mixing, but is accompanied by high total-pressure losses and does not provide any thrust from the fuel jet momentum. Parallel injection, on the other hand, minimizes the stagnation pressure losses and has the added advantage of providing additional thrust from the fuel. The major disadvantage of unenhanced parallel injection is that it suffers from slow mixing layer growth. In fact, both theoretical and experimental research by several authors[2,3] has shown up to a fourfold decrease in the spreading rate of a supersonic mixing layer with increasing Mach number when compared to an incompressible mixing layer. These studies confirm that it is very difficult to achieve high levels of mixing between parallel supersonic streams without some form of enhancement. Several techniques have been, and continue to be, investigated to enhance this slow mixing associated with parallel injection. The combination of two general classes of mixing enhancement schemes, the application of swirl to the fuel jet and shock-induced vorticity, form the basis for the current study.

Based on studies performed at subsonic and transonic speeds, Swithenbank and Chigier[4] postulated that substantial increases in mixing rates could be realized by injecting the fuel jet with swirl. Several experimental studies[5–9] have demonstrated that a substantial increase in mixing rate, mixing layer growth, jet plume area, and mixing efficiency is obtained by parallel or angled injection of a swirling fuel jet into a supersonic stream of air. Naughton and Settles[6] and Cutler et al.[8] offer the possibility that the generation of turbulence associated with vortex breakdown provides a mechanism for the mixing enhancement. Vortex breakdown, observed in supersonic flow as a result of a vortex interacting with either a normal[10] or an oblique shock[11,12] is characterized by an abrupt expansion of the vortex core, the generation of a reversed flow region, and a stagnation point on the axis of the vortex. In a supersonic combustor, the breakdown-induced reversed flow region could serve as a flame holder with the added advantage of being located away from the walls and, thus, alleviating problems with high heating.

A class of injectors designed to augment mixing by the intersection of a fuel jet with an oblique shock was proposed and studied by Marble et al.[13,14] and Waitz et al.[15] The underlying principle of this design is to generate a strong streamwise component of vorticity, also called baroclinic vorticity, at the interface of the low-density fuel and high-density air by the pressure gradient of the oblique

Received 24 August 1998; revision received 3 July 1999; accepted for publication 21 July 1999.

*Graduate Research Assistant, Department of Aerospace Engineering; currently Research Engineer, United Technologies Research Center, 411 Silver Lane MS 129-20, East Hartford, CT 06118. Senior Member AIAA.

†Professor, Department of Aerospace Engineering. Associate Fellow AIAA.

shock. Vorticity is deposited at every point where the density and pressure gradients are misaligned, as the shock passes through the jet. The oppositely directed vorticity tears the fuel jet apart into two counter-rotating vortices, whose sense is such that the fuel migrates in the direction of the shock. The induced vorticity provides a significant amount of mixing enhancement, and the rate of change of vorticity ω is given by

$$\rho \frac{\mathrm{D}}{\mathrm{D}t}\left(\frac{\omega}{\rho}\right) = \frac{1}{\rho^2}\nabla p \times \nabla \rho \tag{1}$$

Shock impingement produced a noticeable increase in fuel/air interfacial area, resulting in improved mixing. In addition, excellent penetration of the fuel into the mainstream has also been reported, with the fuel jet completely lifting off the wall within one injector height for some cases.[15] Drummond[1] performed numerical calculations on fuel/air mixing and the combustion of a circular hydrogen jet and a parallel coflowing stream of air enhanced by an oblique shock and reported a significant increase in mixing and combustion efficiency for the shock-enhanced case. It was further observed that the heat release from the chemical reactions was effective in breaking down the stable hydrogen vortex pair that provided additional mixing and combustion.

Previous numerical calculations by Nedungadi and Lewis[12] investigated the interaction of a streamwise vortex with an oblique shock in air, to study the fundamental aspects of oblique shock/vortex interactions (OSVI) and to explore the flowfield properties in detail not available through experiment. It was found that, depending on the conditions of the vortex, the OSVI resulted in a significant redistribution of vorticity that could possibly be used to enhance supersonic mixing. In the present study, the streamwise air vortex is replaced with a swirling helium jet, to model low-density hydrogen, and is allowed to interact with an oblique shock. The objective is to investigate, in a nonreacting flow, the degree of mixing enhancement that can be achieved when the low-density fuel jet is injected with swirl and allowed to interact with an oblique shock. Figure 1 presents a schematic of this flowfield showing the physical and computational coordinate systems that are used. The helium jet, modeled as a vortex, is injected at Mach 3, parallel to a coflowing stream of air at Mach 4, and is allowed to interact with and pass through an oblique shock generated by a two-dimensional wedge of angle $\theta_s = 20$ deg. Three different vortex strengths are used to study the effects of swirl on mixing enhancement, and the results are compared to the baseline case involving a jet with no swirl. Table 1 lists the cases considered and the vortex properties of the swirling jets. In Table 1, S and τ are parameters used to characterize the strength of the vortex in terms of nondimensional quantities.

An important parameter in evaluating the mixing performance of injectors is the jet-to-freestream pressure ratio. For example, a given

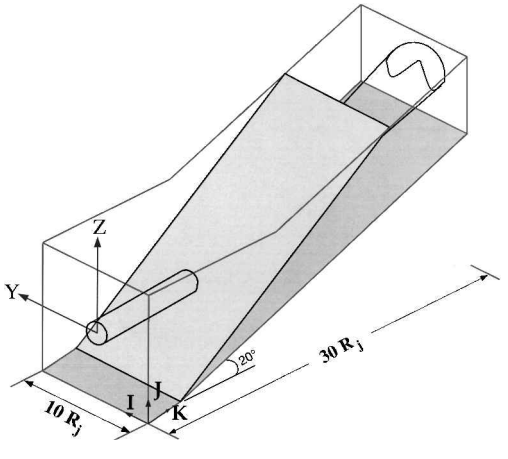

Fig. 1 Flowfield schematic of OSVI showing physical and computational coordinate systems.

Table 1 Test matrix and other properties

Case	Γ_0, m^2/s	r_c	$\bar{P}_{j,\mathrm{axis}}$	$\bar{V}_{j,\mathrm{axis}}$	S	τ
1	0.0	——	1.0	1.2	0	0
2	0.801	3.05	0.7	1.1	0.164	0.117
3	0.856	3.30	0.8	1.1	0.162	0.115
4	1.457	3.56	0.5	1.1	0.256	0.182

Table 2 Injectant and freestream properties

Case	$\bar{P}$	R_j, mm	$\dot{m}_j$, kg/s	$\dot{m}_\infty$, kg/s	q
5	1.0	9.00	0.228	13.35	0.628
6	0.5	12.49	0.226	12.92	0.325
7	2.0	6.78	0.227	13.53	1.086

fuel mass flux can either be injected through small injectors at high pressure or through large nozzles at low pressure. For normal or angled injection from a combustor wall, a high-pressure jet is necessary to penetrate the thick boundary layer. In fact, when investigating the angled injection of helium at 15 and 30 deg, it was reported that the mixing performance increased as the jet/freestream pressure ratio was increased.[16] On the other hand, Waitz et al.,[15] in their analysis of parallel injection of helium through a contoured wall injector, concluded that an injectant/freestream pressure ratio of less than one provided the most effective mixing performance. Clearly, the better mixing performance achieved by lower pressure, lower momentum jets will have to weighed against two issues: first, a larger injector required for given fuel mass flux and, second, less thrust available from the lower momentum jets. The second objective of this work is to investigate the effects of jet-to-freestream pressure ratio $\bar{P}$ on the mixing performance. Table 2 lists the properties of the jet and the freestream of the cases considered in this work. The baseline case $\bar{P} = 1.0$ has an injector radius $R_{j,1} = 0.009$ m. To maintain the same injectant mass flow, $R_{j,2} \approx \sqrt{(2)} R_{j,1}$, whereas $R_{j,3} \approx R_{j,1}/\sqrt{2}$.

The freestream pressure of both the jet and air are taken to be 1 atm, whereas the freestream density of the air and jet are 1.277 and 0.593 kg/m^3, respectively. At these conditions, the jet and air velocities are calculated to be 1600 and 1333 m/s, respectively. The radius of the helium jet $R_j = 0.009$ m, and the wedge angle $\theta_s = 20$ deg. The values of r_c for each of the vortices, M_∞, M_j, and R_j corresponded to the values used by Naughton et al.[7] in their experimental work involving the parallel injection of helium into air without the interaction with a shock. The values of Γ_0 used in the current study are chosen to match the vortex strengths of the experimental work as closely as possible.

The evaluation of the mixing performance of each of these cases is based on several parameters that include the decay of maximum helium mass fraction, the fraction of injector area occupied by the helium jet at $c_{\mathrm{He}} \geq 0.95$, the fraction of total helium mass flux present at various mass fractions, an integral measure of the change in vorticity, termed enstrophy, and the rise in total entropy as well as that due to mixing. A detailed explanation and the significance of these parameters is deferred to the Results section.

Numerical Technique

The laminar, parabolized Navier–Stokes (PNS) equations are used as the governing set of equations. The PNS equations can be used satisfactorily in this case because the core inviscid flow is supersonic everywhere in the domain and there is no streamwise flow separation. In addition, it is assumed that the streamwise viscous and energy diffusion terms are negligible compared to those in the transverse direction. In comparison to the full Navier–Stokes (NS) equations, the PNS equations offer great savings in computational time, as well as decreased memory requirements. The parabolic–hyperbolic nature of the equations allows the space marching of the solution in the streamwise direction.

Table 3 Size and minimum grid spacing for the computational grids

Designation	Size (i dim × j dim × k dim)	ΔX, m	$\Delta Y = \Delta Z$, m	No. of points in vortex core	No. of points in fuel jet
Fine	121 ×121 ×201	1.35×10^{-3}	3.95×10^{-4}	19	49
Medium	91 ×91 ×151	1.80×10^{-3}	5.09×10^{-4}	15	37
Coarse	61 ×61 ×101	2.70×10^{-3}	7.90×10^{-4}	10	25

Numerical solutions of the PNS equations are obtained using GASP 3.0 (Ref. 17). GASP solves the three-dimensional integral form of the time-dependent, Reynolds averaged NS (RANS) equations, as well as the subsets of the RANS equations including the PNS and Euler equations, and is formulated as a cell-centered, finite volume, upwind-biased code.

The inviscid flux vectors at the cell centers are calculated using Van Leer's flux vector splitting with second-order accuracy implemented in the crossflow and streamwise directions. In regions with large gradients, for example, near shocks, it is necessary to perform some limiting of the higher-order corrections to maintain stability and reduce spurious oscillations in the solutions. To this end, Roe's Superbee limiter was used in the present investigation because it provides the least amount of numerical oscillations near the shocks and minimizes the diffusion of the

Second-order central differencing is employed in calculating the gradients in the viscous flux terms. The coefficients of laminar viscosity μ_{l_i} and thermal conductivity k_{l_i} for each individual species are calculated using Sutherland's law. The corresponding mixture values are obtained using Wilke's semi-empirical rule. Finally, the laminar diffusion coefficient $\mathfrak{D}_l$ is calculated as $\rho\, \mathfrak{D}_l = \mu_l / Sc_l$, where Sc_l is the laminar Schmidt number chosen to be 0.7. The diffusion coefficient are assumed to be the same for all species. In the present investigation, the flow and the mixing process are assumed to be laminar. Although the use of a turbulence model would produce results that might be closer to reality, the qualitative trends of this study are not expected to change with a laminar flow assumption. The goal is to explore, at least as a lower bound, a potential mechanism for mixing enhancement. From a practical standpoint, because turbulence would introduce more uncertainties than useful results and because it would have greatly increased CPU requirements and, thus, severely restrict the number of parametric cases run, only laminar flow cases are considered.

An implicit two-factor approximate factorization is also utilized, and the Courant–Friedrichs–Lewy number is linearly ramped from a value of 1 to 10 to accelerate the convergence. The solution in each plane is considered to be converged when the residual decreased by at least six orders of magnitude, where the residual is essentially a summation of the flux contributions in each of the directions. Each crossflow plane typically required 15–20 iterations to converge with a complete solution requiring approximately 75–85 min on a CRAY J-90.

The GASP code has been used extensively to simulate supersonic mixing and nonmixing flows. Sekar[18] modeled the air-to-air mixing of a Mach 2 freestream with a normal and parallel injected jet at Mach 1.4 and 1.7, respectively. Sekar compared numerical calculations using the Baldwin–Lomax and $k-\epsilon$ turbulence models with experimental data. The numerical solution correctly predicted the essential features of both flowfields. However, both turbulence models had significant difficulty in predicting the eddy viscosity patterns and far-field maximum injectant decay. Srinivasan et al.[19] modeled the normal injection of air into air, 15 deg injection of He into air, and 30-deg injection of H_2 into N_2 and air using GASP with a Baldwin–Lomax turbulence model and seven species, seven reaction chemistry model. Their numerical results compared very well to experimental planar laser-induced iodine fluorescence images data of species concentrations. Nedungadi[20] modeled the interaction of a supersonic streamwise vortex with an oblique shock and compared it to the experimental data of Smart and Kalkhoran.[11] The numerical results showed close agreement to the experiment in terms of surface pressure measurements, as well as to qualitative shadowgraph images.

Computational Grid

A three-dimensional, semi-adapted, algebraic grid is used in this study. The computational mesh was obtained first, by generating a two-dimensional semi-adapted grid in the X–Z plane that was then distributed in the Y direction using a stretching function such that the grid points are clustered around the fuel jet. The grid in the X–Z plane is clustered in the Y direction along an approximate trajectory of the fuel jet.

The effects of grid resolution are studied using three computational grids designated coarse, medium, and fine. The dimensions of the three grids may be found in Table 3. The coarse mesh is obtained from the fine mesh by removing every other grid point in each coordinate direction, whereas the medium grid is constructed with a grid size that is an average of the coarse and fine meshes. The boundaries and regions of grid clustering are preserved for all three grids, and all solutions are obtained on the identical grid to eliminate any numerical differences associated with the grid.

Boundary Conditions

The two side boundaries ($\bar{Y} = \pm 5$) (see Fig. 1) and the lower boundary are modeled as an inviscid wall because it was assumed that the influence of the boundary layer on the mixing characteristics would be negligible. A first-order extrapolation is applied at the top boundary, whereas at the outflow plane ($\bar{X} = 30$), a second-order extrapolation is implemented. To generate the oblique shock over the two-dimensional wedge, the entire inflow plane ($\bar{X} = 0$) is prescribed at the freestream conditions of air. To simulate the injection of the helium jet, however, part of the inflow plane is imposed with the jet properties, and the rest of the inflow plane is prescribed at the freestream conditions of air. In GASP 3.0, this is implemented by prescribing the $\boldsymbol{q}$ at each cell center of the inflow plane. For all cells where $r > R_j$,

$$\boldsymbol{q} = [\rho_\infty \quad 0 \quad V_\infty \quad 0 \quad 0 \quad p_\infty]^T \tag{2}$$

whereas for all cells, where $r < R_j$,

$$\boldsymbol{q} = \begin{cases} [0 \quad \rho_{j,v} \quad V_x \quad V_\theta \sin\theta \quad -V_\theta \cos\theta \quad p_{j,v}]^T & \\ & \text{for a swirling jet} \\ [0 \quad \rho_j \quad V_j \quad 0 \quad 0 \quad p_j]^T & \text{for a nonswirling jet} \end{cases} \tag{3}$$

In Eq. (3), $\rho_{j,v}$, V_x, V_θ, and $p_{j,v}$ are the jet properties obtained from the vortex model and r and θ are the radius and angle from the center of the vortex to the center of a cell, respectively.

Vortex Model

The model provided by Délery[21] is used to represent the distribution of tangential velocity V_θ for the helium jet with swirl. This distribution is qualitatively similar to the classic Burger's vortex profile in which a linear velocity distribution exists within the core of the vortex with an exponential decay toward the outer edges of the vortex. V_θ is expressed as

$$V_\theta(r) = \Gamma_0 / r \left\{ 1 - \exp\left[-1.256 \left(r/r_c \right)^2 \right] \right\} \tag{4}$$

A mapping from (r, θ) to (y, z) is used to obtain the v and w components of velocity from V_θ. The pressure through the swirling jet is calculated from the radial momentum equation,

$$\frac{\mathrm{d}p_{j,v}}{\mathrm{d}r} = \frac{\rho_{j,v} V_\theta^2}{r} \tag{5}$$

assuming the radial velocity is zero. Here, $\rho_{j,v}$ is obtained from the equation of state and assuming that the total temperature is constant. Note that experimental work[8,10] has shown that there is indeed a decrease in total temperature through the vortex, albeit quite small.

Experiments with vortices generated by flow over wing tips[11] and swirl vanes[10] have shown that there also exists a deficit in streamwise velocity V_x across the vortex, with a minimum velocity at the center of the vortex. This deficit in velocity may be a result of the low energy in the boundary layers near the surfaces of the wing or the swirl vanes. In the present work, an axial velocity deficit has also been included using the following function provided by Délery[21]:

$$V_x(r) = V_j + V_j(\Phi - 1)e^{-(r/b)^2} \tag{6}$$

$$\Phi = V_{x,\text{axis}}/V_j \tag{7}$$

In Eq. (6), $\Phi = 0.9$ has been chosen to match $M_{j,\text{axis}}$ reported in the experimental work by Naughton et al.,[7] and $b = r_c$ is assumed. Previous work has shown that this axial deficit has a strong impact on the shock/vortex interactions (SVI).[12]

Results

The effects of swirl and jet-to-freestream pressure ratio on the mixing performance of a swirling helium jet, injected parallel to a supersonic airstream, interacting with an oblique shock are investigated. The effects of swirl are investigated by considering the mixing performance of a jet with no swirl and varying amounts of swirl. The effects of jet-to-freestream pressure ratio is analyzed by investigating pressure ratios of 1.0, 0.5, and 2.0. In addition, the effects of grid resolution on the solution is discussed.

Grid Resolution Study

The effects of grid resolution are studied using the three grids tabulated in Table 3 for the case involving the strongest vortex, case 4. The variation in the solution due to grid size is examined by considering the distribution of helium mass fraction in two crossflow planes, $\bar{X} = 15$ and 30. Figures 2 and 3 show the spanwise distribution of helium mass fraction at $\bar{Z} = 2.2$ and 8.1, respectively. The two $\bar{X}$ planes chosen here are downstream of the helium jet/shock interaction. Downstream of the interaction, the helium jet is split into two counter-rotating vortices, and the two peaks in helium mass fraction, shown in Figs. 2 and 3, correspond to the high concentrations of helium in the two vortices. It can be seen that the c_{He} distribution on the medium grid closely follows that of the fine grid, except that the peak in c_{He} is underpredicted by about 15%. The coarse grid, on the other hand, consistently predicts much lower values than either the medium or fine grids. More detailed comparisons have been performed[20,22] and those results also confirm that the solution on the medium grid is in close agreement to that on the fine grid, whereas the coarse grid is inadequate at capturing the essential details of the flowfield.

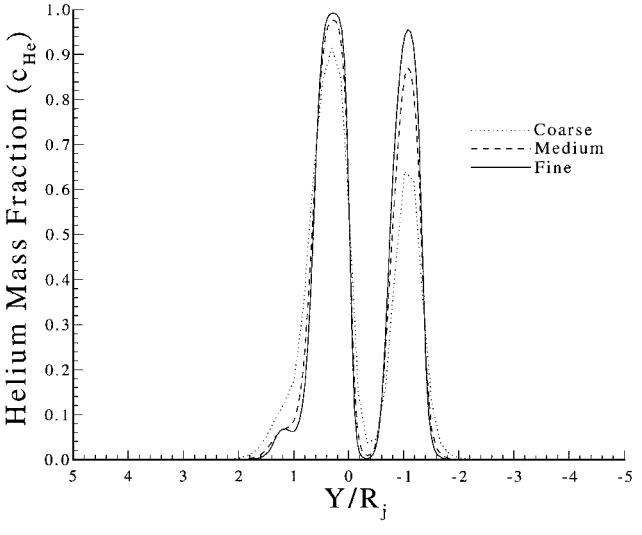

Fig. 2 Variation of helium mass fraction along $\bar{Z}$ = 2.2 in the $\bar{X}$ = 15 plane.

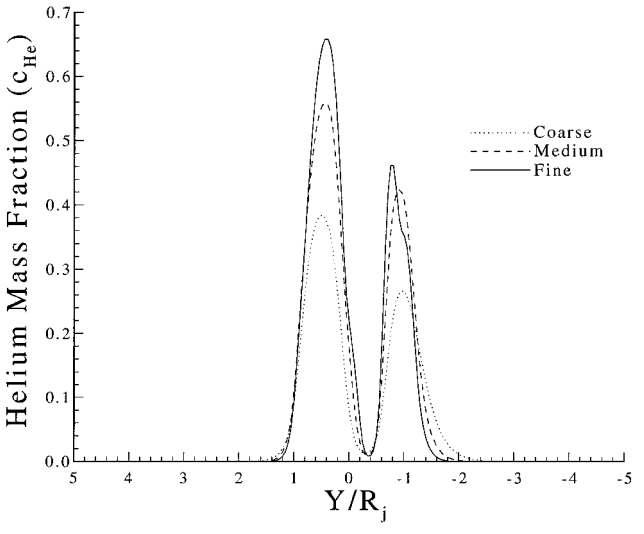

Fig. 3 Variation of helium mass fraction along $\bar{Z}$ = 8.1 in the $\bar{X}$ = 30 plane.

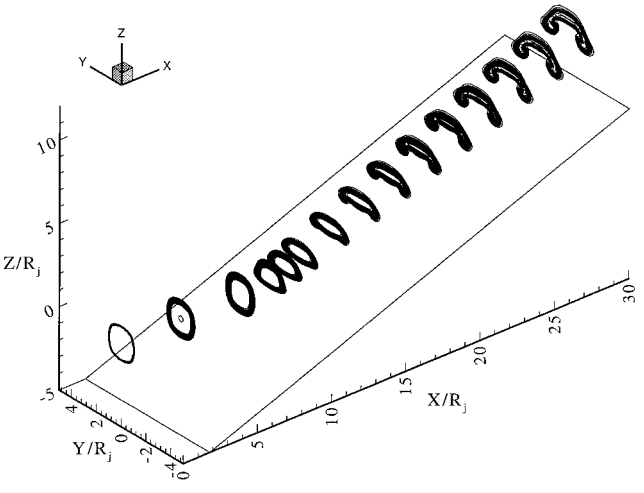

Fig. 4 Helium mass fractions at $\bar{X}$ = 0, 4, 8, 10, 11, 12, 14, 16, 18, 20, 22, 24, 26, 28, and 30 for case 1.

Nonswirling Jet

Case 1 involves a fuel jet with no swirl is selected as the baseline case in this work, and the general characteristics of the flowfield are summarized. Figure 4 presents a contour plot of helium mass fractions at several streamwise stations. As the jet convects downstream of the injection, the jet grows slightly as evidenced by an expansion of the outer edges of the jet. However, as will be shown later, the peak values of c_{He} do not decrease below one for $16R_j$. As the circular jet passes through the shock, it is compressed by the shock and assumes an elongated, elliptical shape. Furthermore, on interaction with the shock, baroclinic vorticity is generated at all of the points in the jet where the density and pressure gradients are misaligned. The baroclinic vorticity quickly coalesces to form two counter-rotating vortices of equal strength. Looking downstream from the inflow plane, the vortex on the negative Y axis rotates clockwise, while the vortex on the positive side of the Y axis rotates counter-clockwise. The fuel jet pair downstream of the interaction is highly symmetric, and the circulation in each plane is zero. The symmetry that is achieved is due to the uniform region within the initial jet. The helium jet deflects upward at roughly the same angle as the rest of the flow downstream of the shock.

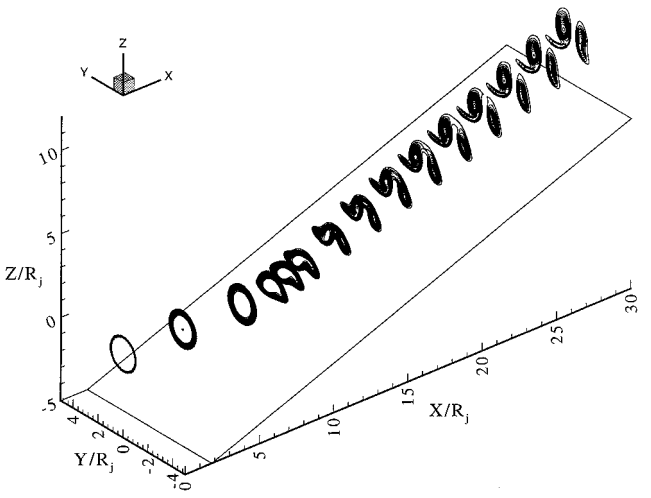

Fig. 5 Helium mass fractions at $\bar{X}$ = 0, 4, 8, 10, 11, 12, 14, 16, 18, 20, 22, 24, 26, 28, and 30 for case 4.

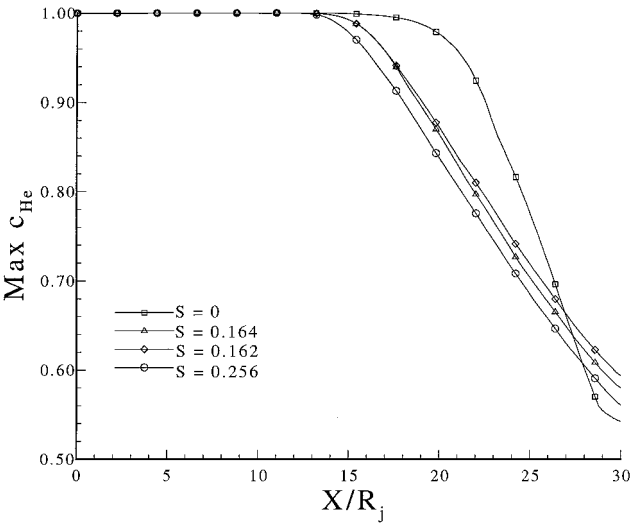

Fig. 6 Effect of swirl on decay of maximum helium mass fraction.

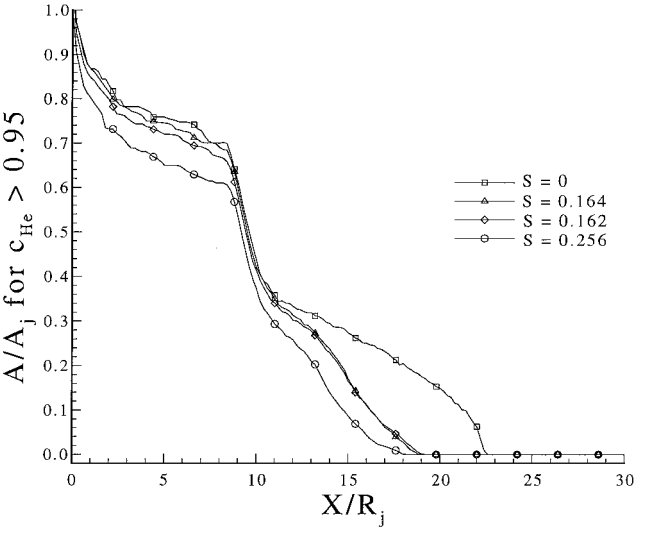

Fig. 7 Area occupied by helium jet at $c_{He} \geq 0.95$.

Swirling Jet

Referring to Table 1, this section presents the general characteristics of the flowfield associated with case 4 and, because cases 2 and 3 are qualitatively very similar to this flowfield, only the mixing performance of those cases will be addressed. A contour plot of helium mass fraction at various axial stations is shown in Fig. 5. As in the nonswirling case, there is a slight expansion of the helium jet, indicating that there is some mixing at the interface of the jet and air due to the shearing between the two fluids. As the jet passes through the shock, it is compressed, taking on a highly irregular shape with most of the compression occurring on the right side of the jet (looking downstream from the plane of injection). The ensuing jet structure is asymmetrical, which is caused by the nonuniform region in the jet that strikes the shock wave at different angles.

As the jet passes through the shock, it is split apart into two counter-rotating vortices. The vortex on the positive side of the Y axis that rotates counterclockwise is much stronger than that on the right. As the vortex on the left rotates, it creates a small tail that gets increasingly stretched out as the vortex convects downstream. The imbalance in the strength of the two vortices causes the jet pair to separate from each other starting at $\bar{X} = 20$. By $\bar{X} = 22$ the two have completely split apart, which is in sharp contrast to the nonswirling case. The complete breakup of the jets results in greater fuel/air interfacial area that in turn should lead to more rapid mixing and combustion.

Mixing Performance

Several parameters have been used to judge the mixing performance of each of the cases. The parameters cast the performance in terms of the degree of mixing enhancement and the total losses by considering the total entropy increase and the increase in entropy due solely to mixing. The mixing enhancement is evaluated by examining the decay of maximum helium mass fraction, the fraction of injector area occupied by the helium jet at $c_{He} \geq 0.95$, the fraction of total helium mass flux present at various concentrations, and an integral measure of vorticity change, termed enstrophy.

Decay of Maximum Helium Mass Fraction

One measure of the mixing performance is provided by the decay of maximum helium mass fraction, calculated by selecting the maximum value of helium mass fraction contained in each Y–Z plane and plotting that against distance downstream of the inflow plane. Figure 6 shows the effect of swirl on the decay of maximum helium mass fraction. For all four cases $c_{He,max}$ remained at unity even after the interaction with the oblique shock. However, $c_{He,max}$ for the swirling jets begins to decrease near $\bar{X} = 13$, whereas for the nonswirling jet the decrease only begins near $\bar{X} = 17$. The $c_{He,max}$ for the nonswirling jet decays at a more rapid rate, and by $\bar{X} = 28$ has lower values of $c_{He,max}$ than for the case with the highest swirl. It appears that the $c_{He,max}$ for the nonswirling jet is leveling off, whereas that for the swirling jet continues to decrease. Cases 2 and 3 have approximately the same values of swirl, and as such, the characteristics of $c_{He,max}$ decay are similar, with case 2 performing slightly better than case 3.

Area Occupied by Helium

Simply calculating the total area occupied by the helium jet can be a misleading parameter because there is no information on the concentration levels of the fuel in that area. In other words, even though the total jet area increases, if a large fraction of that area contains fuel at $c_{He} \approx 1$, combustion will be small. Therefore, it is important, from a combustion point of view, to have fuel at mass fractions that are at or close to stoichiometric values. In this work, the area occupied by the helium jet with mass fractions greater than 0.95 is used, normalized by the area of the original jet A_j.

The area occupied by the helium jet at $c_{He} \geq 0.95$ provides information on the rate at which helium is being convected and mixed downstream of the injection plane, and the effect of swirl on this parameter is shown in Fig. 7. The decrease in area is much more rapid for case 4 than the other three cases. After the jet interacts with the shock, there is a precipitous drop in area indicating that the shock has a significant effect on the mixing performance. It can be seen from Fig. 7 that the point at which there exists no pure helium is reached by $\bar{X} = 18$ for the jet with the highest swirl, whereas the nonswirling

jet reaches this point by $\bar{X} = 22.5$. This indicates that for the nonswirling jet there exists helium at $c_{He} \geq 0.95$ for a longer distance downstream of the injection plane than for the swirling jet cases.

Enstrophy: Change in Vorticity

In the present problem, three phenomena can contribute to the overall change in vorticity: generation due to baroclinic vorticity, the redistribution due to compression, and the generation of vorticity due to a curved shock. Recall that, in the cases with swirl, the vortex induces a curvature in the shock near the region of the interaction. Enstrophy is an integral measure of the change in vorticity and is expressed as

$$E = \iint \bar{\omega}_x^2 \, d\bar{A} \tag{8}$$

where the vorticity ω and area A are nondimensionalized by V_∞ / R_j and A_j, respectively.

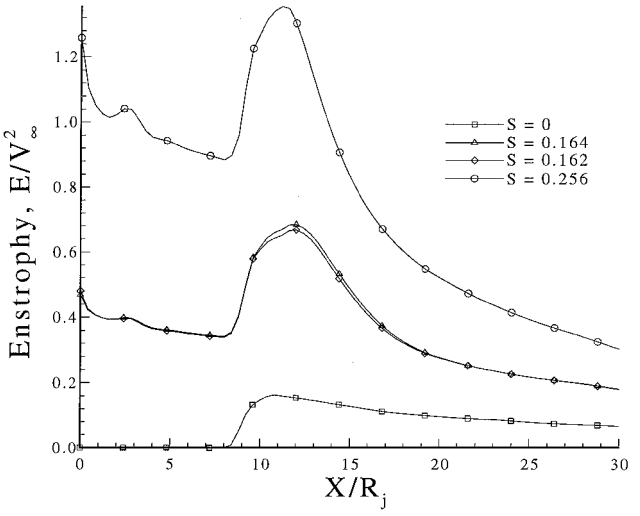

Fig. 8 Effect of swirl on the variation of enstrophy in the streamwise direction.

The enstrophy parameter is calculated at each axial station using Eq. (7), and its variation in the streamwise direction is shown in Fig. 8. As expected, the enstrophy for the no-swirl jet is zero until the interaction with the shock. At this point, the enstrophy increases because of the generation of baroclinic vorticity and remains fairly constant thereafter. The cases involving swirl, however, start with some initial value of enstrophy that decreases slightly until the jet interacts with the shock. The decrease is due to the viscous dissipation of the vortex. When the jet interacts with the shock, there is a large increase in enstrophy. The reason for the larger enstrophy rise, in comparison to the nonswirl case, is due to the additional vorticity created by the curved shock, as well as a significant redistribution of vorticity.

Although the decrease in enstrophy for the swirling jets is more rapid, the level of enstrophy is consistently higher than for the nonswirling jet. The large rise in enstrophy for the swirling jet should contribute significantly to the rapid mixing in the near field, whereas the sharp decrease in enstrophy probably results in the decreased mixing rate much farther downstream of the shock.

Mixedness Measure

A mixing measure that determines the fraction of total helium mass flux present at various concentrations at each axial station, $\dot{m}_{He}/\dot{m}_{He\text{-}total}$ vs c_{He} vs $\bar{X}$, is used in this study to evaluate the mixing performance of each of the cases.[15] This measure reveals the amount of helium (fraction of total injected helium mass flux) that is present at various concentrations (mass fraction) as a function of distance from the injection plane. At each axial plane, varying amounts of helium will exist at various mass fractions. For example, at the injection plane, all of the injected helium exists in its pure state, that is, $c_{He} = 1$, whereas for a well-mixed case, there should be larger amounts of helium at lower concentrations at the exit plane. Note that at each axial plane, the integrated amount of helium at all concentrations is equal to the total helium injected. As discussed before, to achieve high levels of combustion, more of the fuel must be present at lower mass fractions (≤ 0.05) as the jet travels downstream.

This mixing measure is displayed as a three-dimensional surface plot in Fig. 9 for case 4, the maximum swirl jet. From Fig. 9, it can be seen that at the inflow plane, all of the helium mass flux occurs

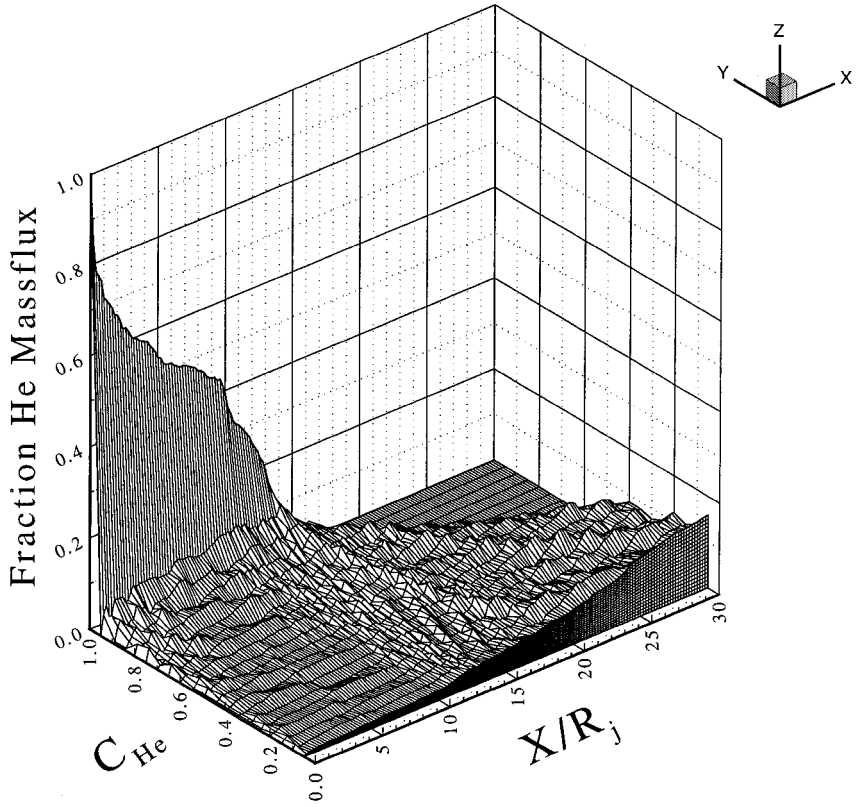

Fig. 9 Mixing measure for case 4, maximum swirl.

at $c_{He} \geq 0.95$, and downstream of the injection plane, progressively larger fractions of the injected helium mass flux appears at the lower mass fractions. For the nonswirling jet, only 8% of the total helium mass flux exists at $c_{He} \leq 0.05$, whereas for the jet with maximum swirl, the fraction of mass flux at that concentration is 16%. A large fraction of the helium mass flux exists in the range of $c_{He} = 0.4$–0.6 for the nonswirling jet. The fraction of helium mass flux existing at $c_{He} \leq 0.05$ is shown in Fig. 10 for all of the cases. From Fig. 10, it can also be seen that the addition of swirl not only increases the fraction of helium mass flux present at $c_{He} \leq 0.05$, but also results in a more rapid rate of increase.

Entropy Rise

In addition to evaluating the performance of the various cases based on mixing effectiveness, it is also important to assess the losses that are incurred. The losses that accompany all mixing enhancement schemes fall into three basic categories: losses that do not augment mixing, losses due to phenomena that enhance mixing, and the thermodynamic losses directly associated with mixing losses. The increase in entropy due to mixing is inevitable, and because it occurs strictly due to mixing, represents an unavoidable tradeoff, though there must be a compromise between the losses generated and how much mixing enhancement is provided. All other losses should be minimized, to maximize the overall efficiency.

In the present work, the total entropy rise and the entropy rise associated with mixing are calculated for each of the cases. The change in entropy, referenced to that at the injection plane, is shown in Fig. 11. Up to $\bar{X} = 12$, the increase in entropy for all of the cases is nearly the same; however, downstream of this point, the swirling jet experiences slightly higher levels of entropy than the nonswirling jet. The change in entropy due to mixing is also approximately the same for all cases until $\bar{X} = 12$. Downstream of this point, the entropy rise is greater for the swirling jet than for the nonswirling jet. This trend also indicates that the addition of swirl increases mixing. Note that approximately one-third of the total entropy rise is due solely to the mixing of the two gases. The contribution of entropy rise due to the boundary layers has not been considered.

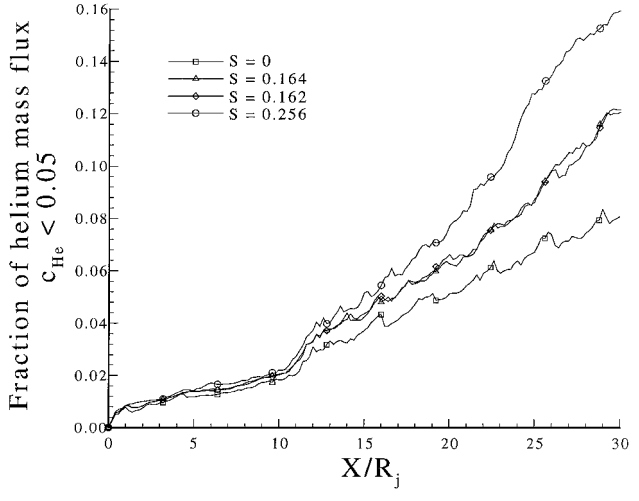

Fig. 10 Fraction of helium mass flux at $c_{He} \leq 0.05$.

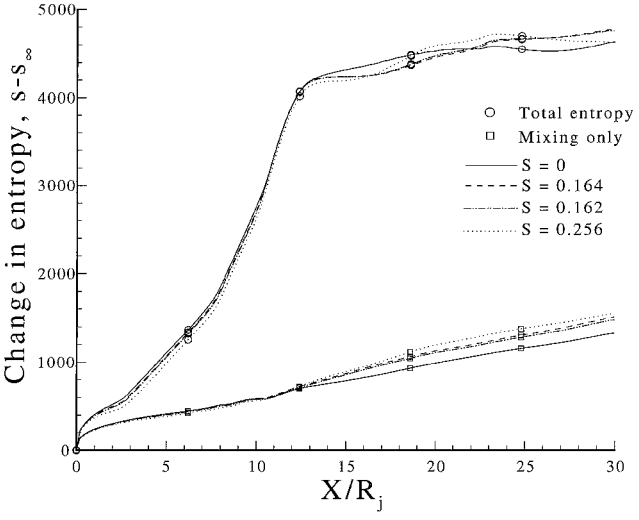

Fig. 11 Change in total entropy and entropy due to mixing.

Effects of Jet-to-Freestream Pressure Ratio

Contour plots of helium mass fraction in the Y–Z plane at $\bar{X} = 0$, 10, 20, and 30 are shown in Figs. 12 and 13 for $\bar{P} = 0.5$ and 2.0, respectively. After passing through the shock, vorticity is deposited along the swirling jet–air interface, and after some distance downstream of the shock, the jet splits apart into two counter-rotating vortices. As a consequence of this, more air is entrained by the jet, resulting in increased mixing.

The vortex on the positive side of the Y axis rotates counterclockwise, whereas that on the negative side rotates clockwise. As the vortex on the left rotates, it creates a small tail that gets increasingly stretched out as the vortex convects downstream. This is only observed for the $\bar{P} = 1.0$ and 2.0 cases. Because of an imbalance in the strength of the two vortices, these individual vortices separate from each other. For the $\bar{P} = 0.5$ case, the separation of the jet pair occurs around $\bar{X} \approx 20$, whereas at the same location, the jet pair in the $\bar{P} = 2.0$ case has not separated completely.

The vortex in the $\bar{P} = 2.0$ case decreases in strength as it convects downstream. The decrease in the peak tangential velocity is caused by the high-pressure jet expanding radially outward. The vortex for the $\bar{P} = 0.5$ case, on the other hand, maintains its strength. As a result, the subsequent SVI is weaker for the $\bar{P} = 2.0$ than for the $\bar{P} = 0.5$ case.

Mixing Performance

Decay of Maximum Helium Mass Fraction

Figure 14 shows the effect of the jet-to-freestream pressure ratio on the decay of maximum helium mass fraction. Although the helium jet intersects the shock at $\bar{X} \approx 8.5$, $c_{He,max}$ decreases below unity only after $\bar{X} \approx 15$. It appears that the formation of the counter-rotating jet pair enhances the diffusion of the injectant. Mass fraction $c_{He,max}$ decays more rapidly for the $\bar{P} = 0.5$ case than for the $\bar{P} = 2.0$ case, and by the exit plane the former case results in a lower $c_{He,max}$ value than the latter one. At the exit plane ($\bar{X} = 30$), $c_{He,max} = 0.53$, 0.58, and 0.68 for $\bar{P} = 0.5$, 1.0, and 2.0, respectively. The splitting of the fuel jet occurs earlier for the $\bar{P} = 0.5$ case, allowing increased diffusion of the helium jet. Waitz et al.[15] observed that for $\bar{P} = 0.4$, the decay of $c_{He,max}$ was more rapid than for $\bar{P} = 4.0$.

Jet Plume Area

The area occupied by the helium jet at $c_{He} \geq 0.95$ provides information about the rate at which helium is being convected and mixed downstream of the injection plane. It also identifies the point at which there is no longer any pure helium in the flowfield. The effect of pressure ratio on this parameter is shown in Fig. 15. The initial area of the jet for the $\bar{P} = 0.5$ and the 2.0 is approximately twice and half that of the baseline case, respectively. In other words, $A/A_{ref} \approx 2$ for the $\bar{P} = 0.5$ case, and $A/A_{ref} \approx 0.5$ for the $\bar{P} = 2.0$ case. Although the rate of decrease in jet area for the $\bar{P} = 0.5$ case is much more rapid than either the $\bar{P} = 1.0$ or 2.0 cases, the area at which $c_{He} \geq 0.95$ is consistently greater. This is expected because the initial jet area for the $\bar{P} = 0.5$ case is greater. For this reason, Fig. 15 can be misleading in that it appears as though the $\bar{P} = 2.0$ case performs better than either of the other two cases. Nondimensionalizing the area by the initial jet area, that is, A/A_j, is more informative.

Figure 16 shows the streamwise variation of A/A_j for $\bar{P} = 0.5$, 1.0, and 2.0. Here, the jet area in which $c_{He} \geq 0.95$ for the $\bar{P} = 2.0$ case actually increases for a short distance downstream of the injection plane and then gradually decreases. The increase in jet

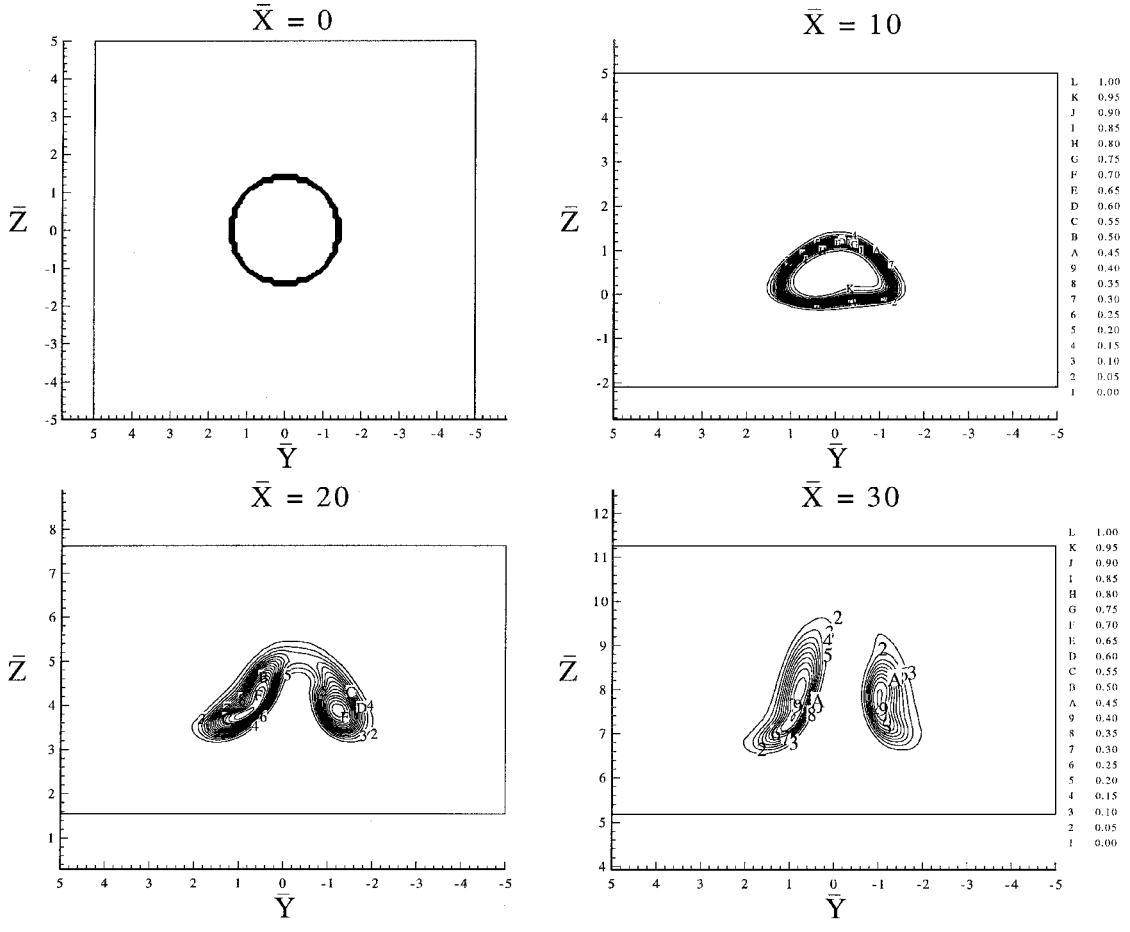

Fig. 12 Contour plot of helium mass fraction at $\bar{X}$ = 0, 10, 20, and 30 for $\bar{P}$ = 0.5.

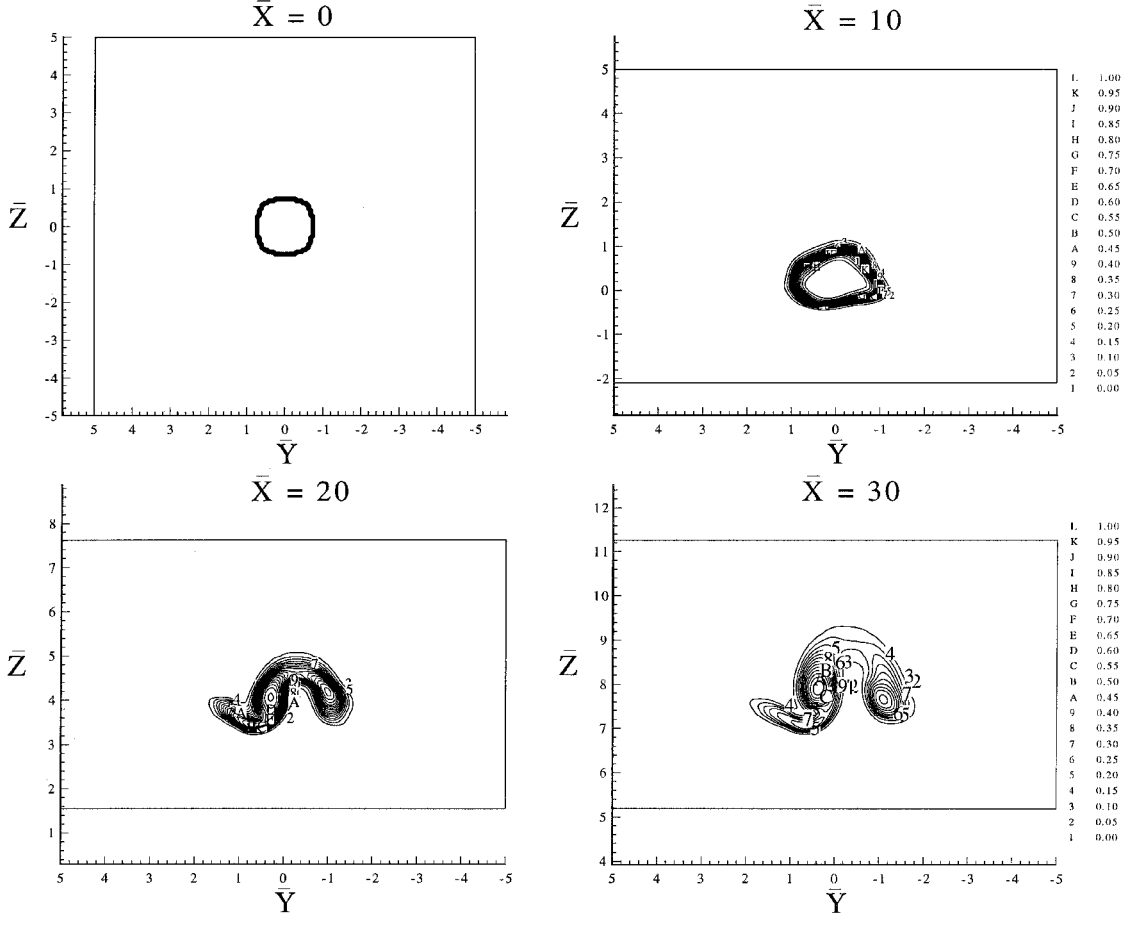

Fig. 13 Contour plot of helium mass fraction at $\bar{X}$ = 0, 10, 20, and 30 for $\bar{P}$ = 2.0.

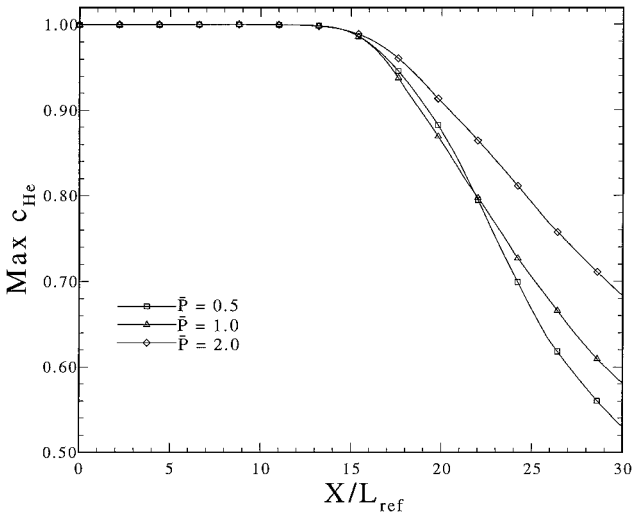

Fig. 14 Effect of jet-to-freestream pressure ratio on the decay of maximum helium mass fraction.

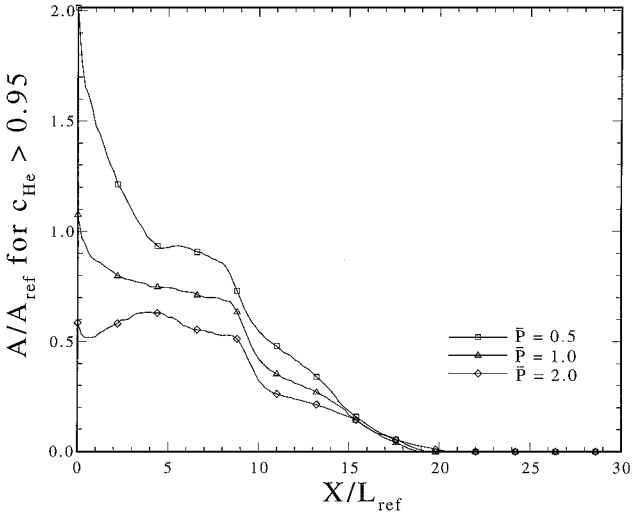

Fig. 15 Nondimensional area of helium jet at $c_{He} \geq 0.95$ for $\bar{P}$ = 0.5, 1.0, and 2.0.

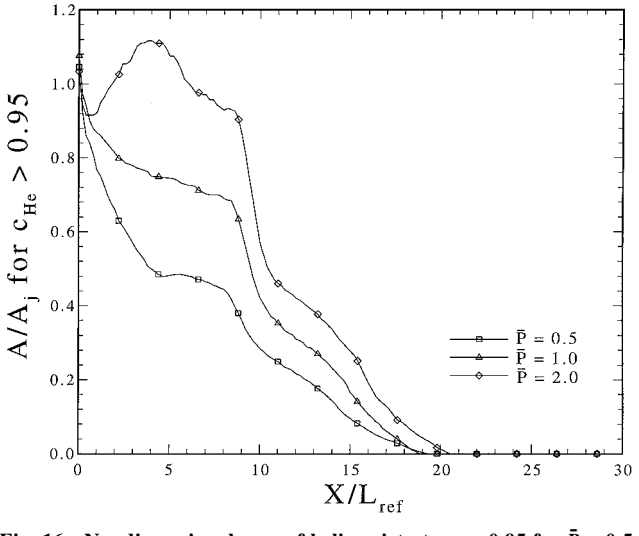

Fig. 16 Nondimensional area of helium jet at $c_{He} \geq 0.95$ for $\bar{P}$ = 0.5, 1.0, and 2.0.

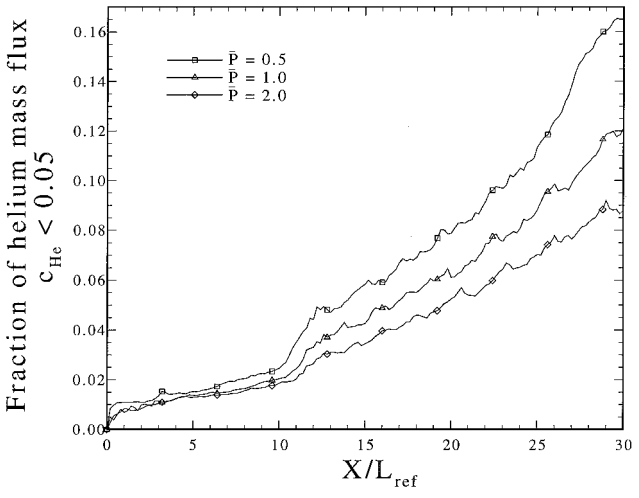

Fig. 17 Fraction of helium mass flux at $c_{He} \leq 0.05$ for $\bar{P}$ = 0.5, 1.0, and 2.0.

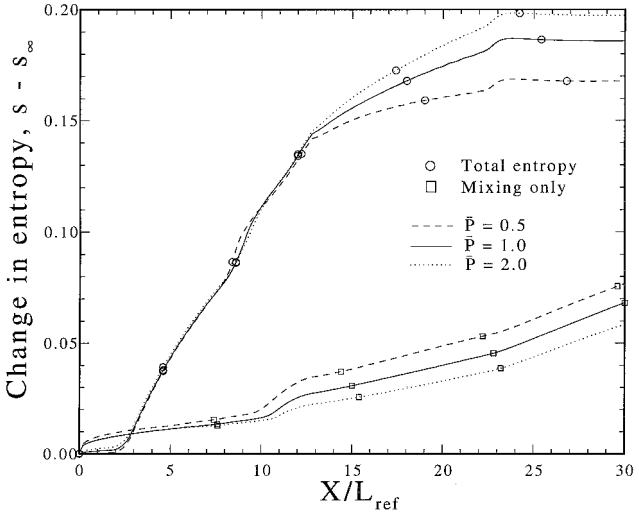

Fig. 18 Variation of total entropy and entropy due to mixing for $\bar{P}$ = 0.5, 1.0, and 2.0.

area is expected because the high-pressure jet tends to expand radially outward. For the $\bar{P} = 1.0$ and 0.5 cases, the area decreases steadily until there is no pure helium in the system by $\bar{X} \approx 20$. Note that the point at which pure helium ceases to exist is roughly the same regardless of the jet pressure.

Mixedness Measure

At the inflow plane, all of the helium mass flux occurs at $c_{He} \geq 0.95$, and downstream of the injection plane, progressively larger fractions of the injected helium mass flux are present at lower mass fractions. At the exit plane, the fraction of injected helium that is present at $c_{He} \leq 0.05$ is 16, 12, and 8% for $\bar{P} = 0.5$, 1.0, and 2.0, respectively. The effect of jet pressure on the mass flux is shown in Fig. 17. Although the injected helium mass flow is the same for all three cases (see Table 2), the $\bar{P} = 0.5$ case results in better mixing than the $\bar{P} = 1.0$ and the 2.0 cases. The reason is that the vortex strength for the $\bar{P} = 2.0$ case decreases considerably before interacting with the shock, thus reducing the mixing enhancement. Essentially, the weaker the vortex, the weaker the interaction is, for a given shock strength.

Entropy Rise

The mass averaged entropy and the entropy due to mixing are shown in Fig. 18. The $\bar{P} = 0.5$ case results in more mixing as evidenced by larger values of s_{mix}. Furthermore, up to $\bar{X} \approx 12$, the total entropy rise is approximately the same regardless of the jet

pressure. Downstream of this point, however, the total entropy for the $\bar{P} = 2.0$ case is higher than for either the $\bar{P} = 1.0$ or 0.5 case. On a loss basis, the lower pressure jet results in more efficient mixing, a conclusion that was also reported by Waitz et al.[15]

Conclusions

This computational study has suggested that the decay of maximum helium mass fraction is more rapid for the swirling jet in the near field. The reason for this seems to be because there is higher vorticity distribution downstream of the shock for the swirling jets. It is found that the increase in entrophy for the nonswirling jet was small. It is observed that the point at which pure helium ceases to exist occurs farther upstream with the addition of swirl. Furthermore, the fraction of total helium mass flux that is present at $c_{\mathrm{He}} \leq 0.05$ increases from 8 to 16% with the addition of swirl. Evaluation based on total entropy rise shows that there is only a small increase in entropy due to swirl; however, the increase in entropy due to mixing alone is found to be higher for the swirling jets.

It is observed that, in the case of the underexpanded jet, the vortex strength of the jet decreases considerably as it convects downstream and, hence, results in a weaker interaction. This occurs because the high-pressure jet tends to expand in the radial direction, and, consequently, the tangential velocity decreases through the vortex. On the other hand, the vortex for the overexpanded case retains its original strength and, thus, results in a stronger interaction as it passes through the shock. As a result of this study, it is believed that mixing performance is greatly increased for lower pressure and momentum jets. Unfortunately the lower momentum jets have two drawbacks:

1) For a given mass flux of fuel, the injector size is larger, leading to increased blockage and increased drag.

2) The thrust provided by the fuel momentum is reduced.

Although it has been shown that the interaction of a swirling jet with an oblique shock can provide increased mixing, it is not clear whether enhanced combustion can also be realized with this method. To evaluate whether the combustion efficiencies are higher with the addition of swirl, a swirling hydrogen jet interacting with an oblique shock must be studied by taking into account the chemical reactions.

Acknowledgments

This work is supported by the Center for Hypersonic Education and Research (NASA NAGw 11796), with Isaiah Blankson as Technical Monitor. The numerical calculations were performed on the Jet Propulsion Laboratory's CRAY Y-MP and J-90. The authors express their appreciation to James E. Randolph for the generous allocation of the CRAY time.

References

[1]Drummond, J. P., "Mixing Enhancement of Reacting Parallel Fuel Jets in a Supersonic Combustor," AIAA Paper 91-1914, June 1991.

[2]Brown, G. L., and Roshko, A., "On Density Effects and Large Structure in Turbulent Mixing Layers," *Journal of Fluid Mechanics*, Vol. 64, No. 4, 1974, pp. 775–816.

[3]Papamoschou, D., and Roshko, A., "Observations of Supersonic Free Shear Layers," AIAA Paper 86-0162, Jan. 1986.

[4]Swithenbank, J., and Chigier, N. A., "Vortex Mixing for Supersonic Combustion," *Proceedings of the 12th International Symposium on Combustion*, Combustion Inst., Pittsburgh, PA, 1968, pp. 1153–1162.

[5]Naughton, J. W., Cattafesta, L. N., and Settles, G. S., "Experimental Study of the Effect of Streamwise Vorticity on Supersonic Mixing Enhancement." AIAA Paper 89-2456, July 1989.

[6]Naughton, J., and Settles, G., "Experiments on the Enhancement of Compressible Mixing via Streamwise Vorticity, Part 1: Optical Measurements," AIAA Paper 92-3549, July 1992.

[7]Naughton, J. W., Cattafesta, L. N., and Settles, G. S., "Experiments on the Enhancement of Compressible Mixing via Streamwise Vorticity, Part 2: Vortex Strength Assessment and Seed Particle Dynamics," AIAA Paper 93-0742, Jan. 1993.

[8]Cutler, A. D., Levey, B. S., and Kraus, D. K., "Near-Field Flow of Supersonic Swirling Jets," *AIAA Journal*, Vol. 33, No. 5, 1995, pp. 876–881.

[9]Kraus, D. K., and Cutler, A. D., "Mixing of Swirling Jets in a Supersonic Duct Flow," *Journal of Propulsion and Power*, Vol. 12, No. 1, 1996, pp. 170–177.

[10]Cattafesta, L. N., and Settles, G., "Experiments on Shock/Vortex Interaction," AIAA Paper 92-0315, Jan. 1992.

[11]Smart, M. K., and Kalkhoran, I. M., "Effect of Shock Strength on Oblique Shock-Wave/Vortex Interaction," *AIAA Journal*, Vol. 33, No. 11, 1995, pp. 2137–2143.

[12]Nedungadi, A., and Lewis, M. J., "Computational Study of the Flowfields Associated with Oblique Shock/Vortex Interactions," *AIAA Journal*, Vol. 34, No. 12, 1996, pp. 2545–2553.

[13]Marble, F. E., Hendricks, G. J., and Zukoski, E. E., "Progress Toward Shock Enhancement of Supersonic Combustion Processes," AIAA Paper 87-1880, June 1987.

[14]Marble, F. E., Zukoski, E. E., Jacobs, J. W., Hendricks, G. J., and Waitz, I. A., "Shock Enhancement of and Control of Hypersonic Mixing and Combustion," AIAA Paper 90-1981, July 1990.

[15]Waitz, I. A., Marble, F. E., and Zukoski, E. E., "A Systematic Experimental and Computational Investigation of a Class of Contoured Wall Fuel Injectors," AIAA Paper 92-0625, Jan. 1992.

[16]Mays, R. B., Thomas, R. H., and Schetz, J. A., "Low Angle Injection Into a Supersonic Flow," AIAA Paper 89-2461, July 1989.

[17]"General Aerodynamic Simulation Program Version 3 User's Manual," AeroSoft, Inc., Blacksburg, VA, May 1996.

[18]Sekar, B., "Three-Dimensional Computation of Parallel and Non-Parallel Injection In Supersonic Flow," AIAA Paper 95-0886, Jan. 1995.

[19]Srinivasan, S., Bittner, R. D., and Bobskill, G. J., "Summary of GASP Code Applications and Evaluation Effort for Scramjet Combustor Flowfields," AIAA Paper 93-1973, 1993.

[20]Nedungadi, A., "A Computational Study of Oblique Shock/Vortex Interactions and Its Application for Supersonic Mixing Enhancement," Ph.D. Dissertation, Dept. Aerospace Engineering, Univ. of Maryland, College Park, MD, May 1997.

[21]Délery, J. M., "Aspects of Vortex Breakdown," *Progress in Aerospace Sciences*, edited by A. D. Young, Vol. 30, Pergamon Press, Oxford, England, UK, 1994, pp. 1–59.

[22]Nedungadi, A., and Lewis, M. J., "A Numerical Study of Fuel Mixing Enhancement Using an Oblique Shock/Vortex Interaction," AIAA Paper 96-2920, July 1996.